Available online at www.sciencedirect.com
SCIENCE DIRECT®
International Journal of Heat and Mass Transfer 49 (2006) 557–574
International Journal of HEAT and MASS TRANSFER
www.elsevier.com/locate/ijhmt

Numerical simulation of film-cooling concave plate as coolant jet passes through two rows of holes with various orientations of coolant flow

Jr-Ming Miao [a,*], Hong-Ka Ching [b]

[a] Department of Mechanical Engineering, Chung Cheng Institute of Technology, National Defense University, Taoyuan 335, Taiwan, ROC
[b] Graduate School of Defense Science Studies, Chung Cheng Institute of Technology, National Defense University, Taoyuan 335, Taiwan, ROC

Received 24 January 2005; received in revised form 27 August 2005
Available online 18 October 2005

Abstract

Computations are performed to predict the three-dimensional flow and heat transfer of concave plate that is cooled by two staggered rows of film-cooling jets. This investigation considers two coolant flow orientations: (1) the coolant jets were ejected from a straight-blow supply plenum, so the coolant supply plane is parallel to the entrance plane of the coolant jets; (2) the coolant jets were ejected from the cross-blow supply plenum so the coolant supply plane was normal to the entrance plane of the coolant jets. The effects of numerous film-cooling parameters were investigated, including the mainstream Reynolds number, the angular locations of the two-row injections and the blowing ratio. The mainstream Reynolds number, determined by the diameter of the injection hole as the characteristic length, varied from 3440 to 13,760. The blowing ratio ranged from 0.5 to 2.0 with a fixed density ratio of 1.14. Additionally, two angles of injections, 40° and 42°, from the exit plane of the entrance duct are considered. Results are presented as the surface adiabatic film-cooling effectiveness, the temperature distribution and the velocity vector profile. The formation and trace of counter-rotating vortex pairs that result from the interaction between the mainstream hot gas and the cooling jets was clearly exhibited. The laterally averaged film-cooling effectiveness over the concave surface with a straight-blow plenum is slightly higher than that of a cross-blow plenum at all test blowing ratios. Results of this study demonstrate that the blowing ratio is one of the most significant film-cooling parameters over a concave surface.

Keywords: Film-cooling; Concave plate; Coolant flow orientation; CFD; Blowing ratio

1. Introduction

The gas turbine engine is one of the most important inventions in the field of man-made power machines because it provides as much as 1500 kW power output. Engineers who design advanced gas turbine engines seek to increase the ratio of the thrust force to the weight and reduce the fuel consumption. The turbine blades must be functional in severe working environments which the pressure is approximately around 30 atm and the temperature exceeds 1680 °C. The protection of the blades from burn out when they are in direct contacted with the hot gas that streaks from the upstream combustor, must be seriously considered. Coating a thin insulation film on the outer surfaces by the CVD or PVD method to isolate the hot steak; arranging dimples or ribs on the interior flow passages to enhance the internal convection heat transfer, and ejecting coolant jets to form a external protective film on the blades' surfaces by film-cooling all are successful methods used by industry. When the discrete-film-cooling method is applied to protect the gas turbine blades, the configurations of the film-cooling holes must be accurately adjusted to the local thermal loads on the blade's surfaces to maximize the benefit from the dispersed cooling jets.

Analysis of the discrete-film-cooling performance requires an understanding of the fundamental jet-in-crossflow. The jet-in-crossflow problem has been investigated

* Corresponding author.
E-mail address: jmmiao@ccit.edu.tw (J.-M. Miao).

0017-9310/$ - see front matter © 2005 Elsevier Ltd. All rights reserved.
doi:10.1016/j.ijheatmasstransfer.2005.08.026

Nomenclature

BR	blowing ratio
D_c	diameter of coolant pipes
L_c	length of coolant pipes
R	radius curvature
T	absolute static temperature
U	gas velocity
X	streamwise coordinate tangent to surface
Y	coordinate normal to surface
Z	spanwise coordinate tangent to surface

Greek symbols

α	injection angle
η	adiabatic effectiveness $(T_{aw} - T_m)/(T_c - T_m)$
$\bar{\eta}$	laterally averaged film-cooling effectiveness
$\bar{\bar{\eta}}$	area average of film-cooling effectiveness
ρ	gas density

Suffixes

m	mainstream flow
c	coolant flow
aw	adiabatic wall

for over fifty years, and has been discussed by Goldstein [1] and Margason [2]. Numerous parameters affect the cooling performance, such as the blowing ratio, the density ratio of the coolant and the hot mainstream, the free-stream turbulence level, the pressure gradient, the curvature, the cooling hole's geometry, the holes spacing and the row arrangement. The thermal-flow structures, the effectiveness of the adiabatic cooling of the film, and the heat transfer rate for various discrete-hole geometries with flat-plate or constant-curvature models have been documented (i.e. by Saumweber and Schulz [3]). However, an issue that has received a relatively less attention is the impact of coolant flow orientation on the development of the coolant jets, especially for discrete-film-cooling with two staggered rows of holes on a concave surface.

Previous research on film-cooling performance has tended to focused on flat plate models with various injection row arrangements and differently shapes of cooling holes. Exploiting an analogy between heat transfer and mass transfer, Goldstein and Yoshida [4] reported the distributions of the local mass (heat) transfer rate on a film-cooling flat plate with one inclined row of coolant jets. They observed lift-off behavior of the coolant jet when the blowing ratio exceeded a threshold. Using the same model, Goldstein and Taylor [5] further discussed the detail of the local mass transfer rates near the injection holes at various blowing ratios. Jurban and Brown [6] reported the effects of row spacing, holes spacing and compound angle on the effectiveness of film cooling through two rows of round holes. Gostelow et al. [7] and Bons et al. [8] elucidated the effects of mainstream turbulence level and pressure gradient on the film-cooling effectiveness over a film-cooled flat plate. Ligrani and Ramsey [9] demonstrated that the compound angles of the second row of holes could improve the film-cooling performance over a flat plate over that obtained using a simple angle injection configuration.

Although numerous investigations had been experimentally or numerically examined the film-cooling performance over a flat plate, several works, such as those of Schwarz et al. [10], Schwarz [11] and Chen et al. [12] have used the convex or concave model to elucidate the effect of curvature. The lift-off of the coolant jets is such that the film-cooling effectiveness declines as the blowing ratio over the convex surface increases. The effect of the blowing ratio on the laterally averaged film-cooling effectiveness on a flat plate is similar to that on a concave surface. Moreover, Chen et al. [12] demonstrated that the film-cooling effectiveness obtained with compound angle injection exceeds that obtained with simple angle injection on both concave and convex surfaces.

Walters and Leylek [13], Berhe and Patankar [14] and Garg and Gaugler [15] conducted several CFD simulations of thermal-flow problems to understand the mechanism that governs film-cooling performance over a flat plate, a constant-curvature surface and a real film-cooled blade. They reported that the two most significant mechanisms that influence the film-cooling effectiveness were the jetting effect on the windward side of the coolant pipes and the counter-rotating vortex pair flow structure downstream of the jet exit. The jetting effect and the strength of the counter-rotating vortex pair changes with the configuration of coolant supply plenum, as evidenced by the PIV results of Peterson and Plesniak [16] for short-holes, whose length-to-diameter ratios are under unity. Their measured velocity fields at different cross-sections determined that the relative rotational direction of in-hole vortices and the counter-rotating vortex pair downstream of the holes exit is closely related to the coolant plenum configuration.

The objective of this study is to elucidate the impact of the plenum feeding direction and the angular location of the discrete holes on the film-cooling effectiveness over a concave surface with two staggered rows of simple round holes, as determined by using the CFD technique. The mainstream turbulence level fixed at 4% whereas the mainstream Reynolds number based on the diameter of injection holes and varied from 3440 to 13,760. The density

ratio is maintained at 1.14 but the tested blowing ratio is increased from 0.5 to 2.0. This study considers two types of coolant plenum, which are the straight-blow type and the cross-blow type. Earlier studies [16,17] observed a very strong relationship between the feeding direction of coolant flow and the film-cooling performance over a flat-plate model, as governed by the variation of the discharge coefficient at the jet exit and the local jetting effect within coolant pipes. However, most studies in this area are experimental, and few have systematically and numerically investigated both the coolant feed direction and the discrete-hole angular location. Accordingly, the main characteristics of this investigation are as follows: (1) Realistic, discrete-hole film-cooling concave surfaces with two rows of staggered injection coolant pipes, and supply plenum regions are investigated. (2) The effects of the mainstream Reynolds number, the holes' angular location, the blowing ratios and the coolant flow orientation on film cooling effectiveness over a concave surface are investigated. (3) The underlying reasons for these effects are considered with reference to film-cooling effectiveness contours and velocity vectors at the centerline of each coolant pipe and at various cross-stream planes downstream of the holes.

2. Numerical method

2.1. Numerical model and methodology

The discrete coolant jets, forming a thin protective film on surfaces of blade, are drawn from the upstream compressor in an operational gas turbine engine. The coolant flows fed through internal passages with various ribs and dimples. They impinge on the inner surface before turning through a narrow internal plenum in the blade or vane. From the supply plenum, the coolants ejected through several rows of discrete-holes or slots over the external boundary layer against the local high thermal spots on the surfaces of the blade. The coolant feed direction is expected to affect the trajectory and the lateral spreading of the jets as they interact with the hot cross-mainstream. In the literature, most of the coolant supply plenums are of the straight-blow type (Maiteh and Jubran [18]); meaning that the normal vector of the entrance plane of the coolant supply plenum is almost parallel to that of the entrance plane of the coolant-pipes. This study builds another type of plenum, called the cross-blow coolant supply plenum, to discuss the effect of the type of supply plenum on the film-cooling effectiveness over a concave surface. Figs. 1 and 2 schematically depict computational film-cooling concave models with straight-blow type and cross-blow coolant supply plenums, respectively. The distinction between Figs. 1 and 2 is in the coolant supply plenum: the direction of the coolant entrance plane of the cross-blow type is normal to that of the straight-blow type.

This numerical model is a constant-curvature rectangular flow passage with two staggered rows of coolant pipes on the concave side of the duct. Fig. 3 shows the dimensions that describe the concave geometry with cross-blow coolant supply plenum. Notably, the coolant jets fed through two types of supply plenum to elucidate the effect of coolant flow orientation. The flowing passage can be divided into three parts—the rectangular entrance flow region, the constant-curvature test section and the curved recovery region. The cross-section of the entrance plane is 100 mm × 50 mm. The span angle and the "strength of curvature" of the test section of the flow passage are 135° and 86, respectively. Of the two rows of film-cooling holes, the first has five holes arranged at equal intervals and the second has four holes. The two rows are interlaced with each other with an angular location of 3°. The angle between the axis of each cooling hole and the mainstream is 35°, the spanwise angle between the axis and the crossflow direction is 0°. The diameter of the cooling holes (D_c) is 5 mm; the ratio between the diameter of the cooling holes and the length of the cooling pipe (L_c) is 3.5, and the ratio of the length of the centerline of each row to the diameter of the cooling pipe is 3.0. This study tested two angular locations of the first row of coolant pipes on the concave surface, 40° and 42° from the exit plane of the entrance duct, as presented in Fig. 4.

The computational domain incorporates the supply plenum, the HEXA module in the software, ICEM/CFD, used to generate the structured multi-block and the body-fitted grid system. This software allows separate grids to generated for different parts of the flow domain, using an appropriate grid system. In this study, the grid system associated with the parts of the mainstream and the coolant supply plenum is H-type, while the two rows of inclined round cooling pipes constitute an O-type grid system, increasing the orthogonality of the mesh. Figs. 1(b) and 2(b) show a magnified view of the grid of the computational domain with straight-blow and cross-blow coolant supply plenums, respectively. The multi-block topology and high quality of the grid system are clearly observed. Grid sensitivity studies were conducted using the standard k–ε turbulence model and the standard wall function. Grid-independent results obtained with $121 \times 151 \times 81$ nodes in the i, j and k directions of the mainstream test section duct. The cells are refined in the near-wall regions of the curved surface and near the injection hole. The y^+ value in the first cell adjacent to the sample walls is always set below unity, according to the criteria required for the individual near-wall treatment.

This study uses a commercial CFD code based on the control-volume method, FLUENT 6.1.22. The flow is treated as incompressible and steady state and the turbulence fluctuations are governed by the Boussinesq eddy-viscosity assumption. The standard k–ε turbulence model with the standard wall function is used to predict the flow structure and heat transfer over the film-cooling concave surface. The three-dimensional incompressible Reynolds-averaged Navier–Stokes equations are solved by a second-order upwind scheme unrelated to the convective terms, whereas the energy terms are evaluated using a third-order QUICK

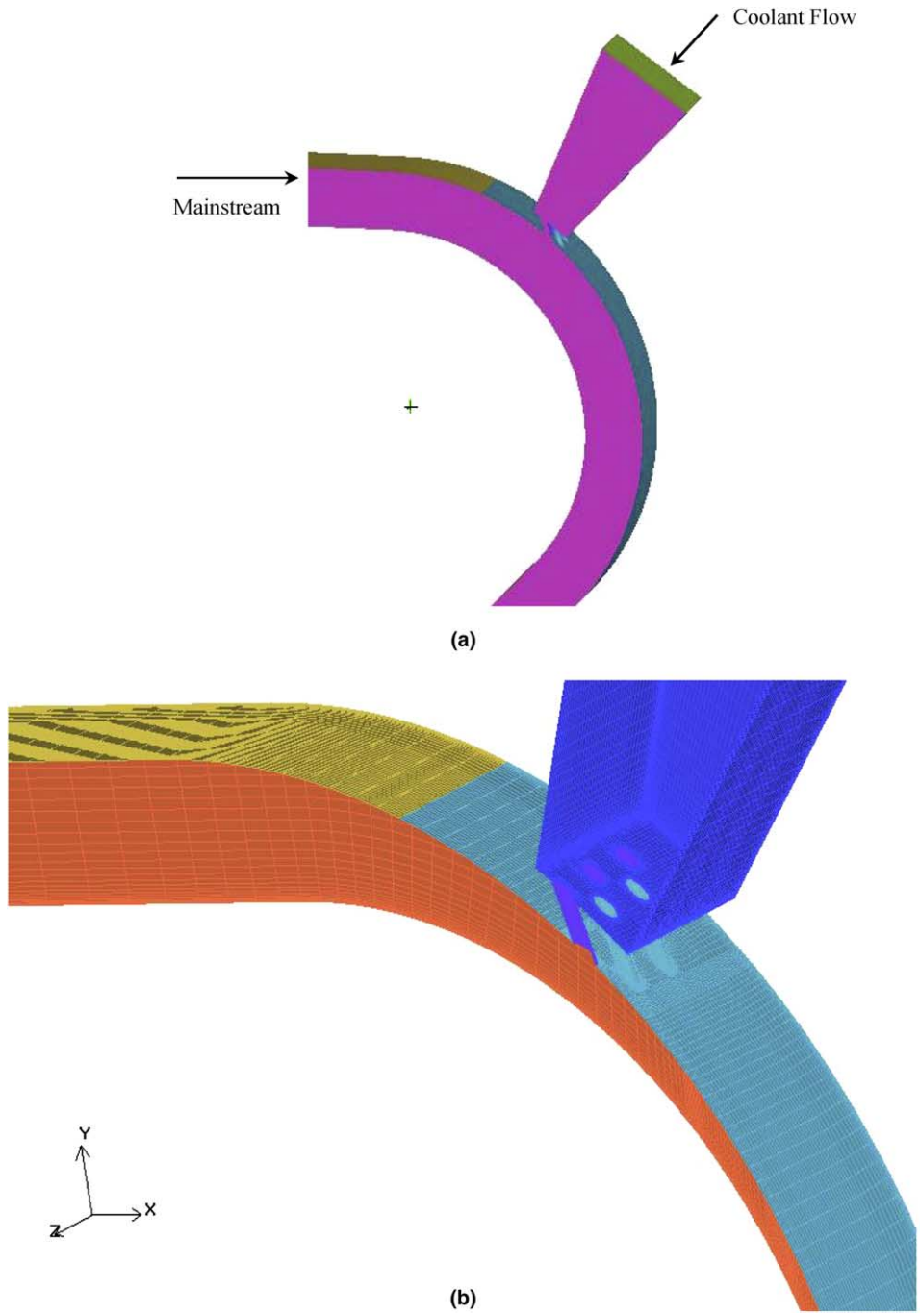

Fig. 1. Computational geometry of film-cooling concave surface with straight-blow supply plenum: (a) solid model, (b) close-view of grid distribution.

scheme. The coupling between velocity and pressure in momentum equations is governed by the SIMPLE scheme. The effect of buoyancy of the coolant jet is proposed by applying Boussinesq's approximation to the density. The mathematical models are described in detail in the FLUENT 6.1.22 Users' Manual. All runs were made on a PC cluster with four Pentium-4 3.2 GHz personal computers connected to an optical host switch hub via optical fiber lines. The convergence criteria of the steady-state solution are judged by the reduction in the mass residual by a factor of 6, typically, in 5000 iterations.

2.2. Operating conditions and test matrix

Fig. 3 displays the types of boundary condition applied in this investigation. The normal speed of the mainstream is set at 10 m/s, 20 m/s and 40 m/s, so the Reynolds numbers that correspond to the diameters of the cooling holes, as characteristic lengths, are 3440, or 6880 and 13,760. The temperature of the mainstream maintained as 333 K, and that of the coolant flow is as low as 293 K, for evaluating the film-cooling performance over a concave surface. Additionally, the turbulence intensity and dissipation length at the inlet

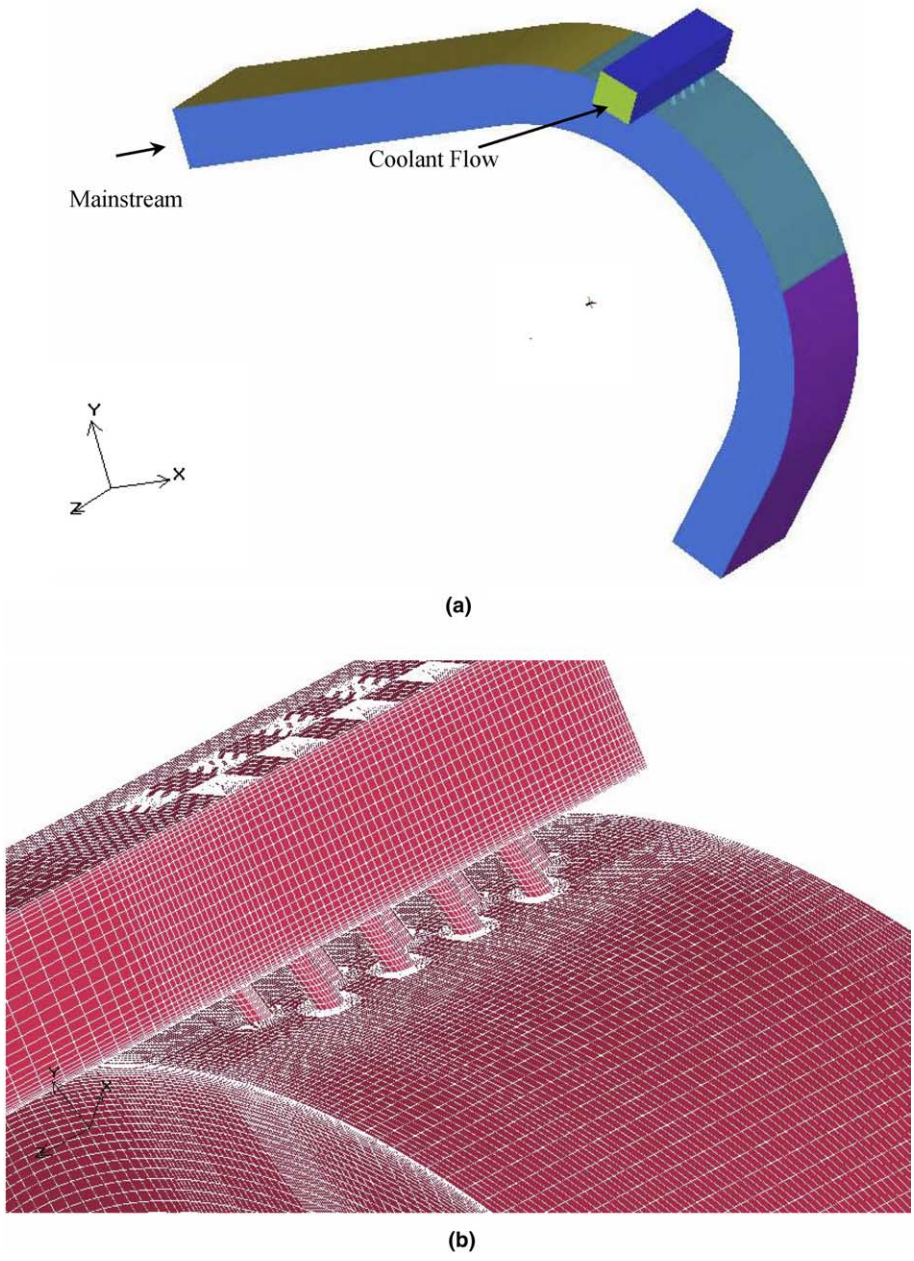

Fig. 2. Computational geometry of film-cooling concave surface with cross-blow supply plenum: (a) solid model, (b) close-view of grid distribution.

boundary of the mainstream are 4% and 15% of the hydrodynamic diameter, respectively. The turbulence intensity at the inlet boundary of the coolant is set to the same value but the dissipation length changed to D_c. The mass flow rate of the coolant is determined by the tested flow parameter—the blowing ratio (BR)—which is defined as follows:

$$\mathrm{BR} = \left(\frac{\rho_c u_c}{\rho_m u_m}\right)_I + \left(\frac{\rho_c u_c}{\rho_m u_m}\right)_{II} \quad (1)$$

where ρ and u represent the density and speed, respectively, the subscripts c and m denote the coolant flow and the mainstream, respectively. The first and second RHS term in the above expression, belong to the first row and second row injections, respectively. The blowing ratios used in this investigation are 0.5, 1.0, or 1.5 and 2.0 with a fixed density ratio of 1.14. The surface boundary conditions of the solid walls are non-slip and adiabatic. The pressure outlet boundary condition specified at the exit of mainstream recovery flow passage. Table 1 presents the computational matrix, including the blowing ratio, the mainstream Reynolds number, the angular location of the two discrete rows of injection holes and the type of coolant supply plenum being tested.

The velocity contours and velocity vectors are shown in various cross-planes, but the computational results are compared by introducing an important non-dimensional quantity—the local adiabatic film-cooling effectiveness which is defined as

$$\eta = \frac{T_{aw} - T_m}{T_c - T_m} \quad (2)$$

where T is the absolute static temperature; the subscript aw denotes the adiabatic wall; c refers to the coolant jets, and m denotes the mainstream.

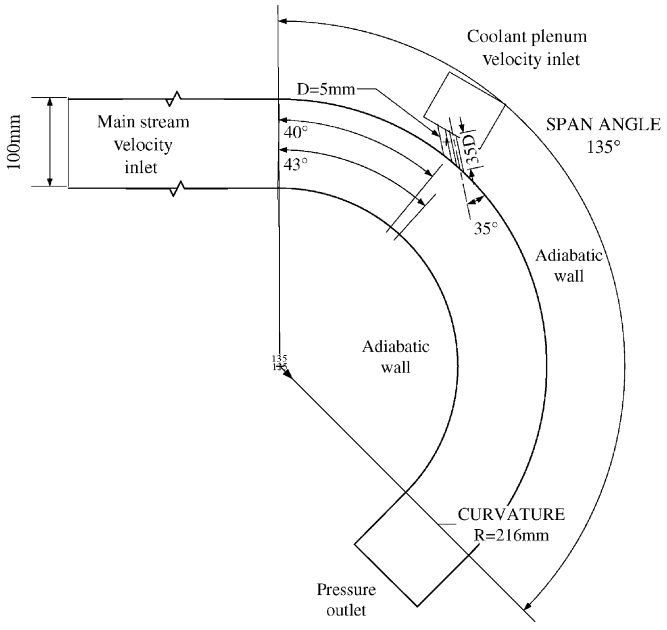

Fig. 3. Schematic of problem with concave wall for model C.

3. Results and discussion

3.1. Comparison with previous studies

Fig. 5 compares the laterally averaged film-cooling effectiveness computed herein as a function of X/D_c for model A with experimental results previously obtained by Chen et al. [12] and numerical results obtained by Berhe and Patankar [14]. The angular locations of the two rows of injection holes are indicated by hollow and solid arrows. To the authors' knowledge, the few computational or experimental results concerning the film-cooling concave surface for two-row injections are available in the literature. Chen et al. [12] performed transient TLC experiments using the same concave-plate model but with only a single row of five injection holes. Berhe and Pantankar [14] numerically investigated a film-cooling concave surface for one and two staggered rows of injection holes, but with a spacing distance that was five times the diameter of the holes between each row.

Fig. 5 demonstrates that adding one row of injection holes significantly increased the laterally averaged film-cooling effectiveness at all blowing ratios—0.5, 1.0 and 1.5—and in particular, at a high blowing ratio. Beyond the downstream location where $X/D_c = 6$, adding one staggered row of injection holes almost doubles $\bar{\eta}$, as stated by Chen et al. [12] at a given blowing ratio. This finding is also consistent with the results in [14].

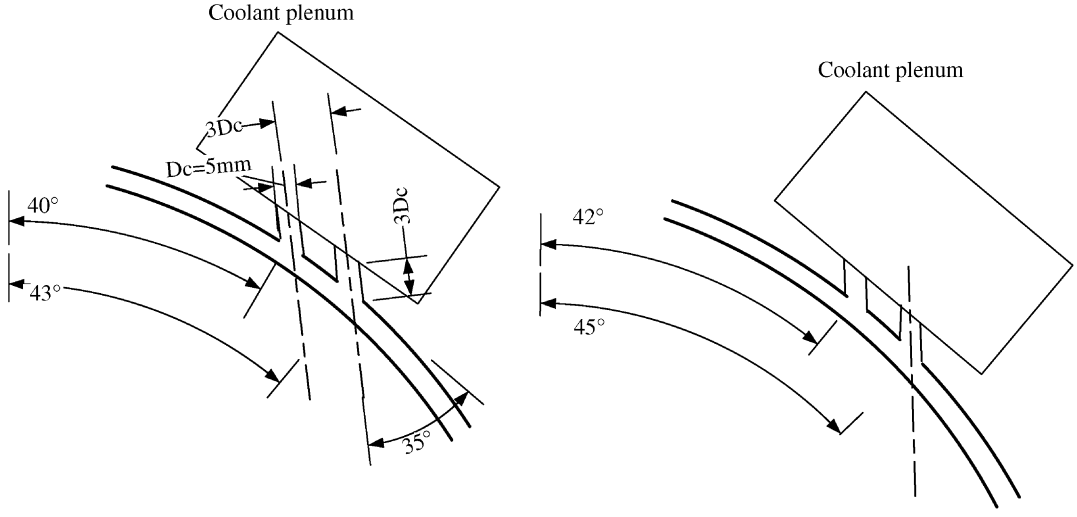

Fig. 4. Schematic view on the angular locations of two-row injections for models C and D.

Table 1
Study matrix

Model	Type of coolant supply plenum	Angular locations of two-rows injections	Reynolds number	Blowing ratio
A	Straight-blow	(40°, 43°)	3440, 6880, 13,760	0.5, 1.0, 1.5, 2.0
B	Straight-blow	(42°, 45°)	3440, 6880, 13,760	0.5, 1.0, 1.5, 2.0
C	Cross-blow	(40°, 43°)	3440, 6880, 13,760	0.5, 1.0, 1.5, 2.0
D	Cross-blow	(42°, 45°)	3440, 6880, 13,760	0.5, 1.0, 1.5, 2.0

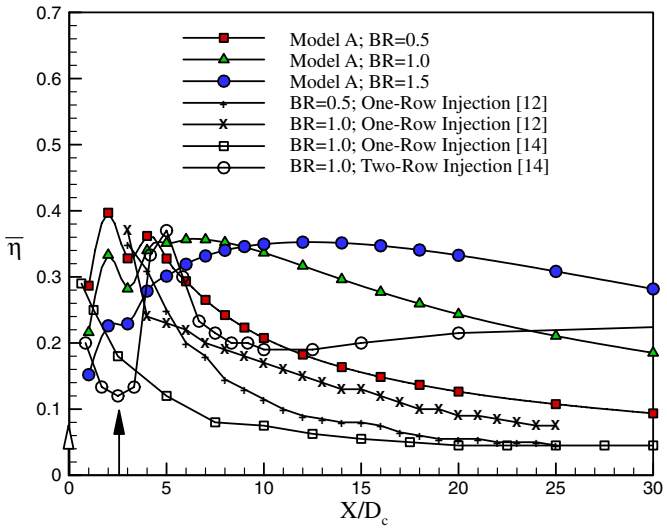

Fig. 5. Comparison between present computed laterally averaged film cooling effectiveness at various blowing ratios for model A with those of Refs. [12,14].

3.2. Characteristics of the flow field

Walters and Leylek [13] and Peterson and Plesniak [16] observed that the pattern of the distributed adiabatic film-cooling effectiveness on the film-cooling surface is dominated by two determined flow mechanisms. The first mechanism is concerned with the local jetting flow structure in the inclined film-cooling pipe. The second mechanism is governed by the shear flow structure, resulting from the interaction between an individual coolant jet and the cross-mainstream. This is called the "jet-in-crossflow" problem. Pairs of counter-rotating vortex dominated the development of the thermal-flow structure over the surface of a discrete-hole film-cooling plate.

Figs. 6 and 7 present the velocity vector field half way along the first row of injection holes with various blowing ratios determined using models B and D, respectively. The mainstream Reynolds number is 6880. These figures reveal two important points. First, when the cooling streams flow into the coolant pipe, the cooling stream may encounter a

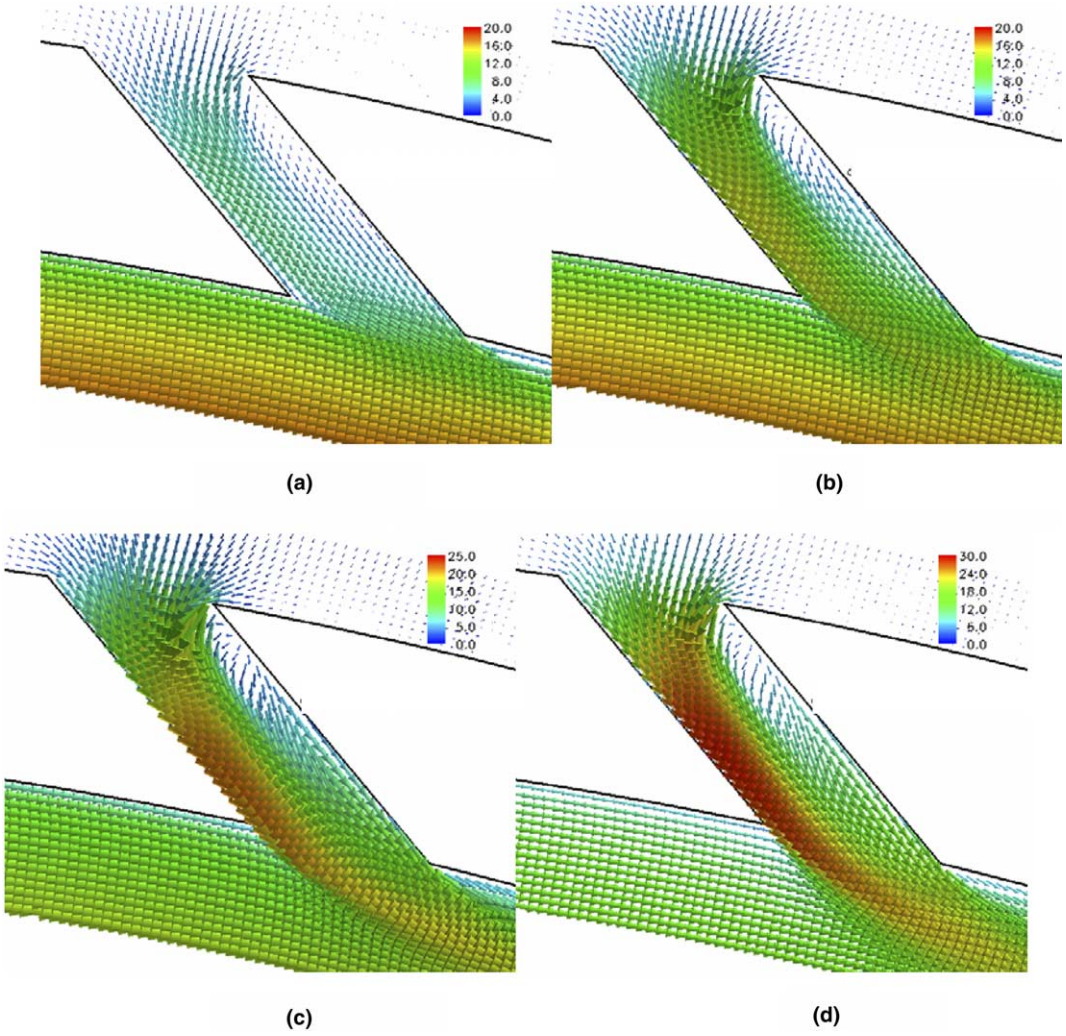

Fig. 6. Velocity vector field along a midway through the first row of injection holes for model B at $Re = 6880$ and (a) BR = 0.5, (b) BR = 1.0, (c) BR = 1.5, (d) BR = 2.0.

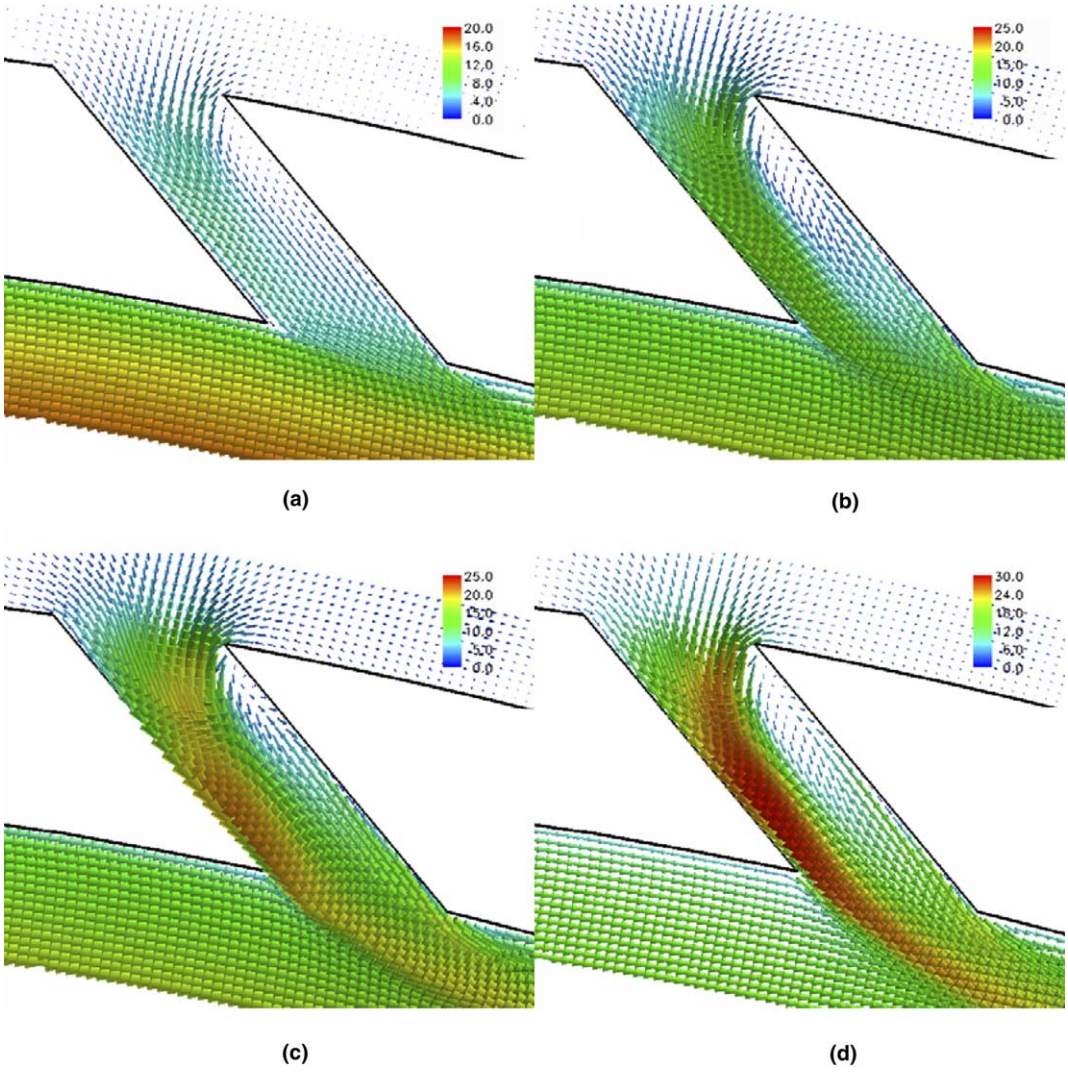

Fig. 7. Velocity vector field along a midway through the first row of injection holes for model D at $Re = 6880$ and (a) BR = 0.5, (b) BR = 1.0, (c) BR = 1.5, (d) BR = 2.0.

larger turning angle near the leeward side of the coolant tube in the upper section, while the majority of cooling stream passes more smoothly into the windward side of the coolant tube. The flow structure of the "jetting effect" formed from the non-even momentum distribution in the entrance plane of the coolant tube. Furthermore, the four parts of the jetting flow-the separated/back flow area near the coolant tube entrance, the re-attachment area, the developing area and jetting exit area near the coolant tube—are affected by the cross-mainstream as demonstrated by the velocity vector plots. When the blowing ratio increased to 2.0, the separated/back flow area in the coolant tube enlarged because the uneven balance of the momentum flux is large at the entrance plane of the coolant hole. The jetting effect enhanced as the blowing ratio increases, so the lift-off of the coolant jet at the upstream leading edge of the hole on the exit plane is more noticeable, as presented in Fig. 8. Additionally, a highly shear layer downstream of the hole exit, formed by the penetration of the coolant stream into the mainstream can be observed when the blowing ratio is increased to 2.0. The peak value of the velocity profile near the upstream edge of the exit plane of the hole at a high blowing ratio, corresponding to the local film-cooling effectiveness, declined rapidly at the near-field of the jet-crossflow intersection, as presented in Figs. 15(c) and 16(c).

The second point is that the variation in the flow structure of the developing coolant jet along the midway through the first row of injection holes is minor in the straight-blow plenum and the cross-blow plenum in the tested range of blowing ratios. Peterson and Plesniak [16] used a model of a film-cooled flat plate that incorporated one row of short-hole injections to determine the flow field within the injection hole was visibly affected by the change in plenum configuration from the co-flow direction to the counter-flow direction. The differences in the effects of the coolant flow orientation on the interior developing jet flow field caused by the difference between the ratios of

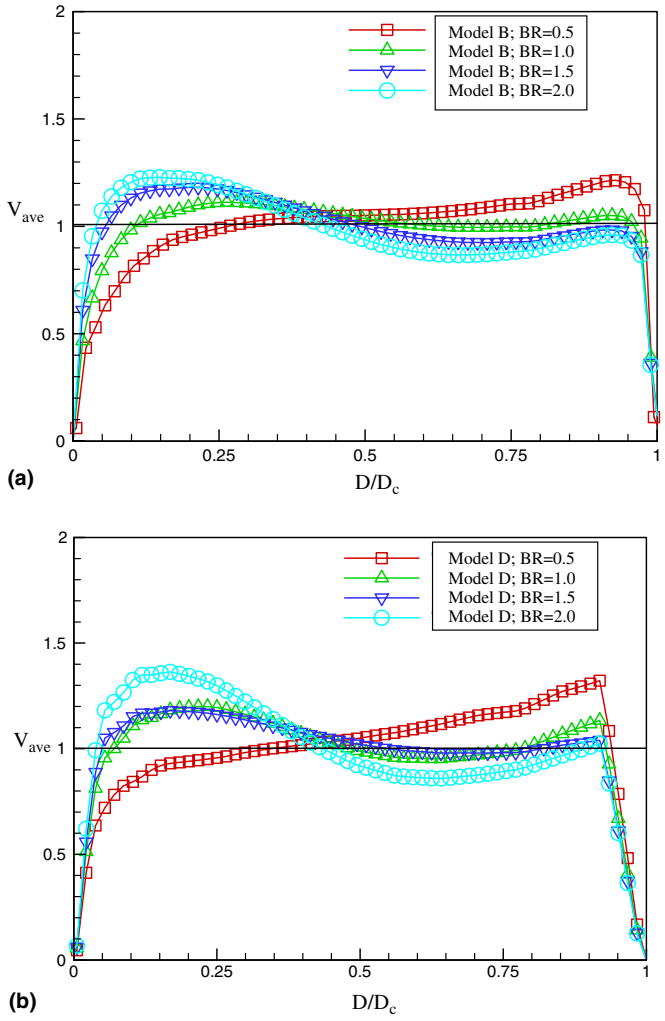

Fig. 8. The effect of blowing ratio on average velocity distribution of the hole exit at $Re = 6880$: (a) model B, (b) model D.

the length of the holes to the diameter of the holes used in each study. The ratio length-to-diameter ratio of the holes in this study was 3.5 attributed, so this investigation involved long holes. The value in the investigation of Peterson and Plesniak [16] was 0.66, so their study concerned short holes. Additionally, the difference between the flow structure of the coolant jet in the second row of injection holes (not shown here) and that in the first row of injection holes is minor in the studies. The developing jets within the coolant tube had similar structures over a range of tested mainstream Reynolds numbers and angular locations of two-row injections.

Figs. 9 and 10 present the velocity field within the first row of injection holes for models B and D, respectively. The mainstream Reynolds number is fixed at 6880. Arrows in both figures indicate the direction of the mainstream, the velocity vector is not scaled in here. Fig. 9(a) reveals that, as the coolant flow enters the injection hole from the straight-blow plenum with a blowing ratio of 0.5, a pair of in-hole vortices occurs around the downstream edge of the holes on the cross-section near the entrance plane with $L/L_c = 0.1$. Midway along the coolant tube ($L/L_c = 0.5$), this pair of in-hole vortices moves toward the central portion of the cross-sectional area and tends to emerge into a single vortex at $L/L_c = 0.7$, when the blowing ratio is 0.5. However, a visibly non-coherent structure of the vortex pair is observed at $L/L_c = 0.7$ at a higher blowing ratio of BR = 2.0 (Fig. 9(b)). On the cross-plane near the exit hole at $L/L_c = 0.9$, the vortical structure is less apparent even when the blowing ratio is as high as 2.0.

Fig. 10 shows that, when the coolant supply plenum is changed from the straight-blow type to the cross-blow type, a single vortical structure around the center portion of the coolant tube at the cross-plane of $L/L_c = 0.1$ dominates the interior flow structure of the in-hole velocity field, regardless of the blowing ratio. The strong vortex core in the central portion biased away from the streamwise centerline. As the coolant flow passes the midpoint of the tube, this single vortical structure tends to separate into a pair of non-coherent vortices. The jetting flow structure forces this pair of vortices to move toward the downstream edge of the holes at the plane for which $L/L_c = 0.7$. Comparing Fig. 10 with the velocity vector field obtained using model B (Fig. 9) demonstrates that the distribution in the interior velocity field is clearly non-uniform at the exit plane in which $L/L_c = 0.9$.

Figs. 11–14 presents the velocity vectors at various locations with various X/D_c location at blowing ratios of 0.5, 1.0 and 1.5 obtained using models A, B, C and D, respectively, at the mainstream Reynolds number of 3440, the velocity vector is not scaled here. The figures clearly showed the counter-rotating vortex pairs (CRVP) generated by the cooling stream ejected from the two rows of injection holes. The intensity of CRVP was amplified by increasing the blowing ratio for all tested cases. Regardless of the coolant supply plenum, the lift-off phenomena of the jets from the first row of injection holes are visible at $X/D_c = 1$ at high blowing ratio. Further downstream at $X/D_c = 5$, the non-coherent CRVP that emerged from the second row of injection holes remained attached to the wall of the concave surface because the oncoming cross-mainstream had been disturbed by the first row coolant flows. The visibly weak CRVP revealed the wide lateral convection of coolant jets and the hot cross-mainstream downstream of $X/D_c = 10$. In this study, the trajectory of the CRVP in the cases with the straight-blow supply plenum differed from that in the case with the cross-blow supply plenum. In the latter case, the size of the CRVP did not obviously change, but lifted higher off the wall at $X/D_c = 5$. This dissimilarity corresponds to the velocity contours at the exit plane of the hole in the straight-blow and cross-blow supply plenum cases (Figs. 9 and 10). The high temperature of the mainstream has an impact on the wall, because of the downwash effect of CRVP, eliminating the equilibrium of the cooling film, so models A and B exhibit better film-cooling performance than models C and D at a given blowing ratio (Fig. 19).

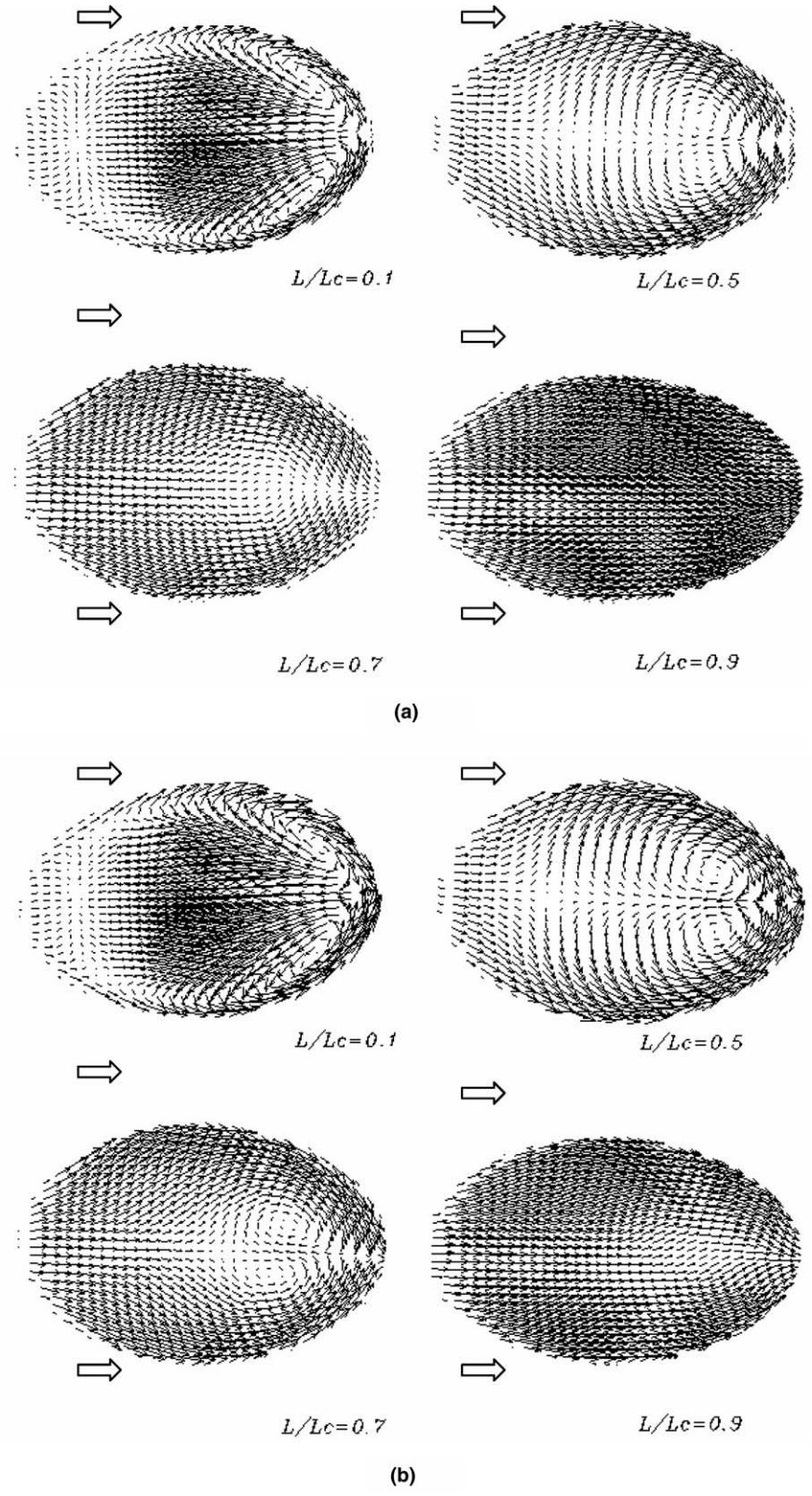

Fig. 9. Evaluation of the velocity field within the first row of injection holes for model B at $Re = 6880$ and (a) BR = 0.5, (b) BR = 2.0.

3.3. Detailed distribution of local film-cooling effectiveness

This investigation numerically analyzes the complicated thermal flow over a film-cooling concave surface with two rows of simple round injections holes. The first and second rows are staggered and separated at an angle of 3°. The angular location of the centerline in the first row of the injection holes is 40° or 42° downstream of the exit plane

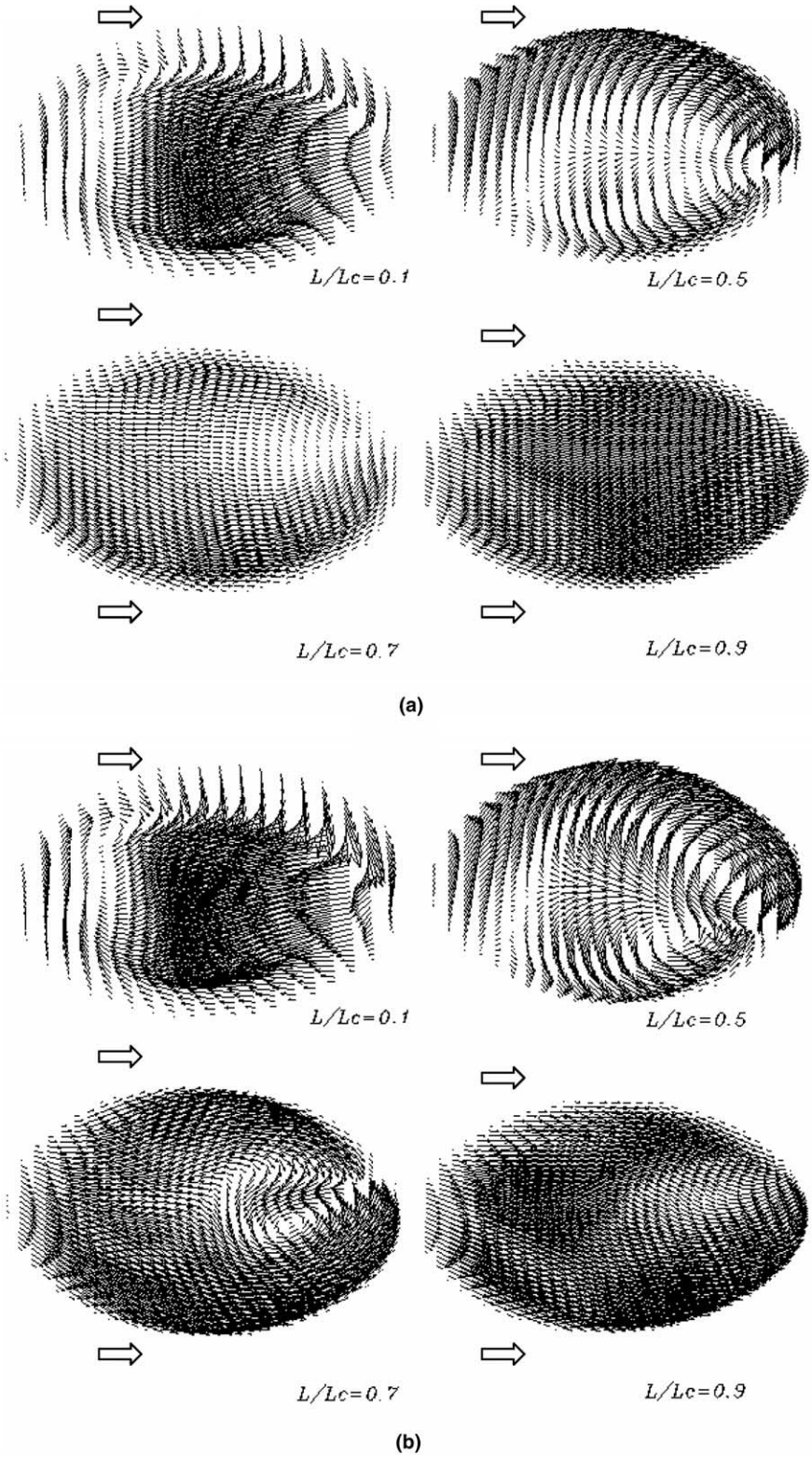

Fig. 10. Evaluation of the velocity field within the first row of injection holes for model D at $Re = 6880$ and (a) BR = 0.5, (b) BR = 2.0.

of the entrance duct. For further comparison and discussing based on computed data, the location of the center of the first row of the cooling holes on the tested concave wall was defined as $X/D_c = 0$, while the location of the center of the second row of the cooling holes on the tested concave wall was defined as $X/D_c = 2.2616$.

Fig. 15 presents the contours of the local cooling effectiveness of the adiabatic film obtained using model A at

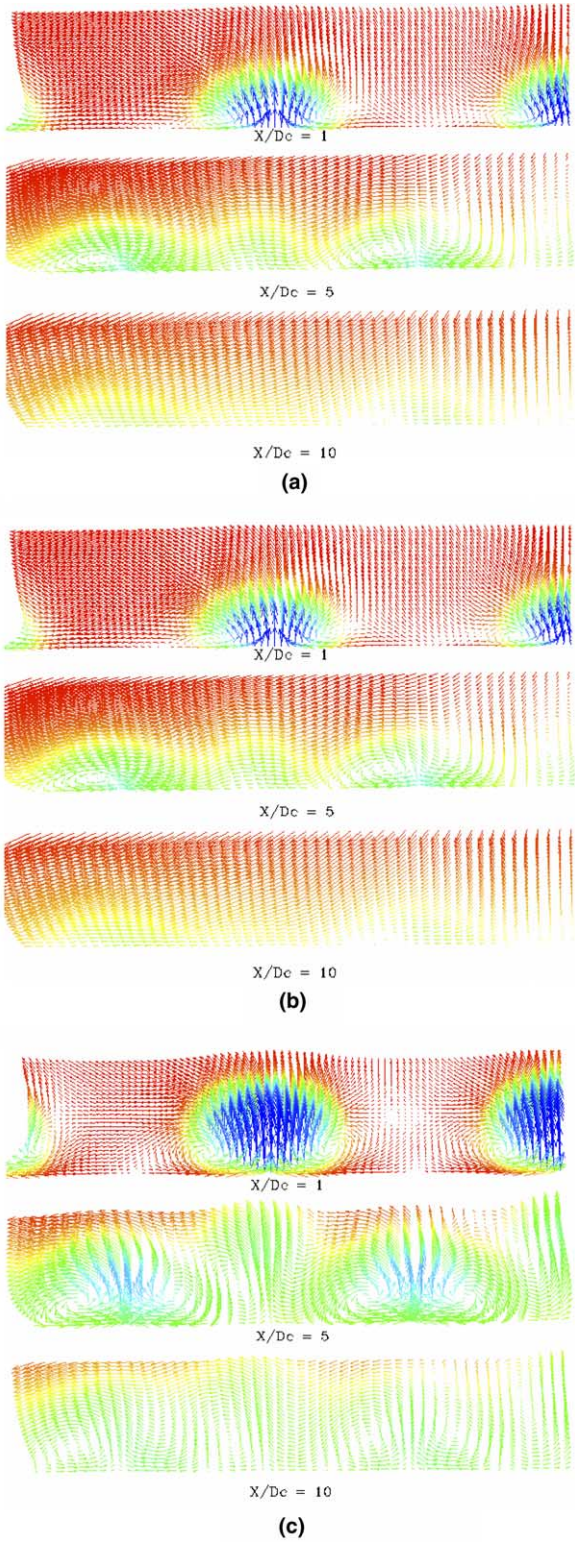

Fig. 11. Effect of blowing ratio on the evaluation of CRVP for model A at $Re = 3440$ and (a) BR = 0.5, (b) BR = 1.0, (c) BR = 1.5.

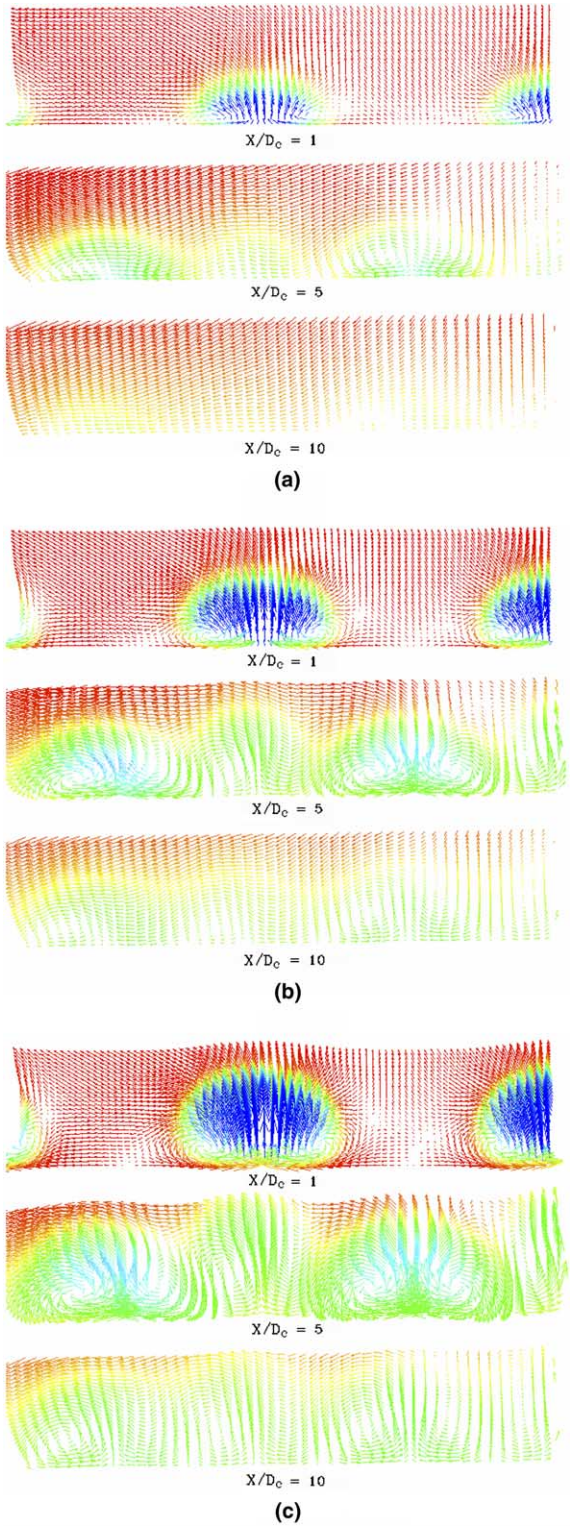

Fig. 12. Effect of blowing ratio on the evaluation of CRVP for model B at $Re = 3440$ and (a) BR = 0.5, (b) BR = 1.0, (c) BR = 1.5.

three blowing ratios—0.5, 1.0 and 1.5—at a tested Reynolds number is 3440. The area covered by the cooling stream is strongly related to the blowing ratio, the lift-off of coolant jets and the strength of CRVP. The downstream regime next to the exit of the first row and the second row of injection holes has a higher η value, but this value gradually declines as the blowing ratio increases, because the coolant jets penetrate far into the boundary layer at high

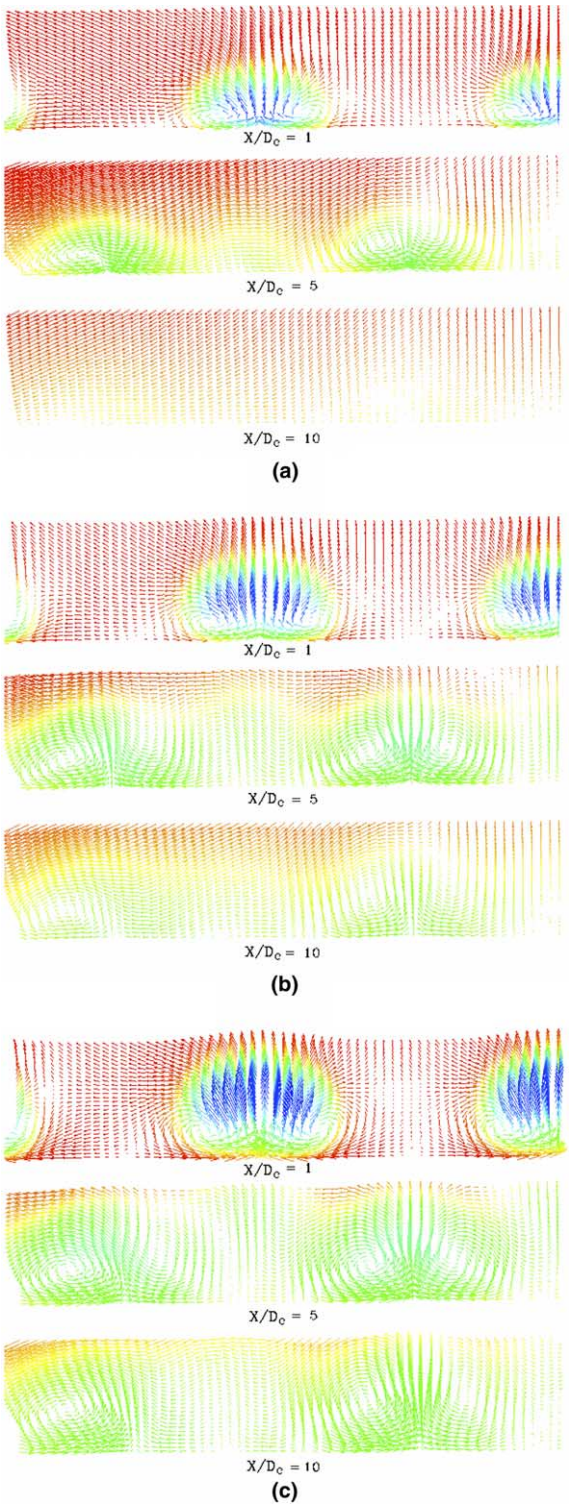

Fig. 13. Effect of blowing ratio on the evaluation of CRVP for model C at $Re = 3440$ and (a) BR = 0.5, (b) BR = 1.0, (c) BR = 1.5.

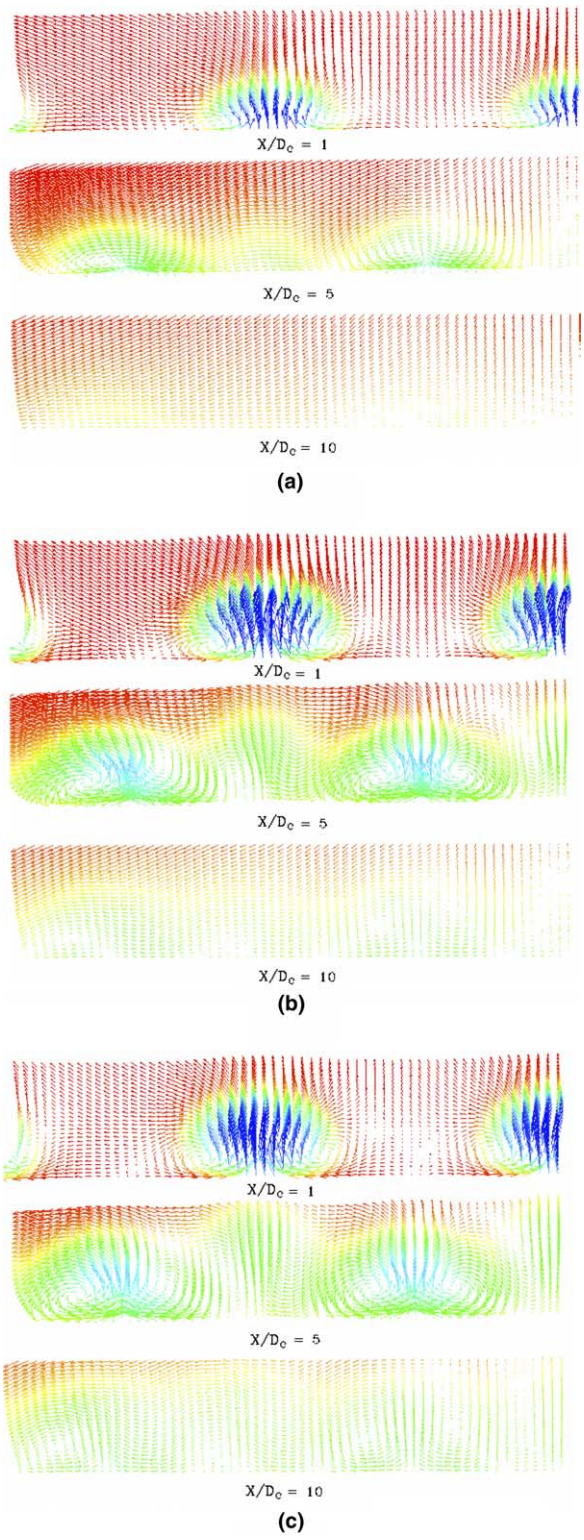

Fig. 14. Effect of blowing ratio on the evaluation of CRVP for model D at $Re = 3440$ and (a) BR = 0.5, (b) BR = 1.0, (c) BR = 1.5.

blowing ratios, especially for the first row of injection holes, as indicated by the exit velocity distributions in Fig. 8. Further downstream, the jetting effect and the strong turbulent shear flow structure on the exit plane of the coolant pipes reduces the size of the visible protection region, which relates to the streamwise movement and the coolant stream ejected from the discrete holes, yielding a η distribution with triangular-like. The simulated results reveal that, in the area around the first row of injection holes, the lower η value covers the main section, indicating that the present simple round hole structure cannot provide

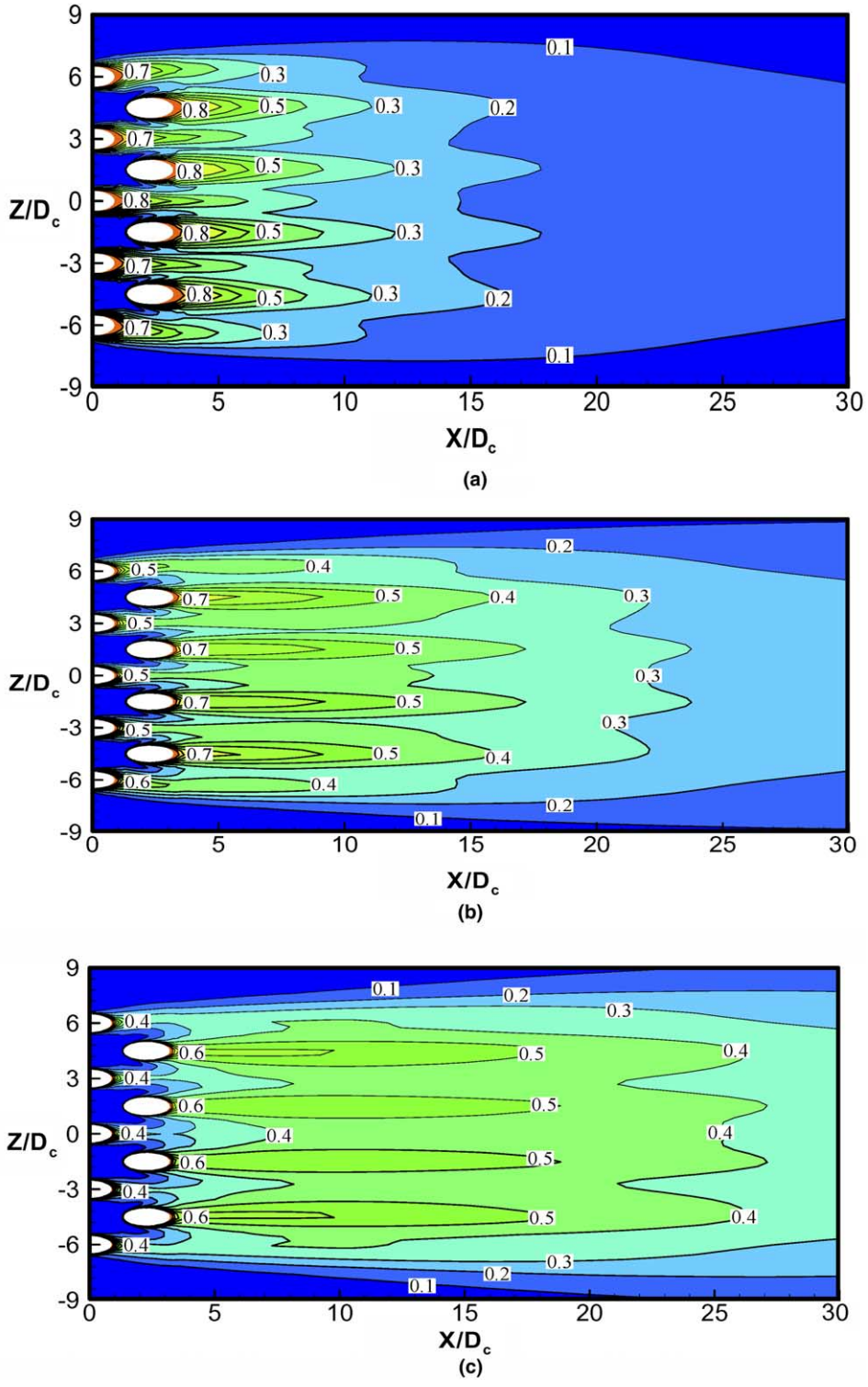

Fig. 15. Effect of blowing ratio on the contours of local adiabatic film cooling effectiveness with model A at $Re = 3440$ for (a) BR = 0.5, (b) BR = 1.0, (c) BR = 1.5.

a better cooling effect in the lateral direction. The staggered arrangement provides better cooling protection in the downstream area of the second row of injections. When the blowing ratio is unity or higher, the original lift-off coolant jets are reattached to the concave surface, improving the cooling performance downstream of $5 < X/D_c < 30$.

Fig. 16 presents similar results on the effect of the blowing ratio on the distributions of the local film cooling effectiveness using a cross-blow supply plenum. A slightly asymmetrical distribution of the local film-cooling effectiveness near cooling holes in the same row is observed because the cooling stream induced from the lateral side, then

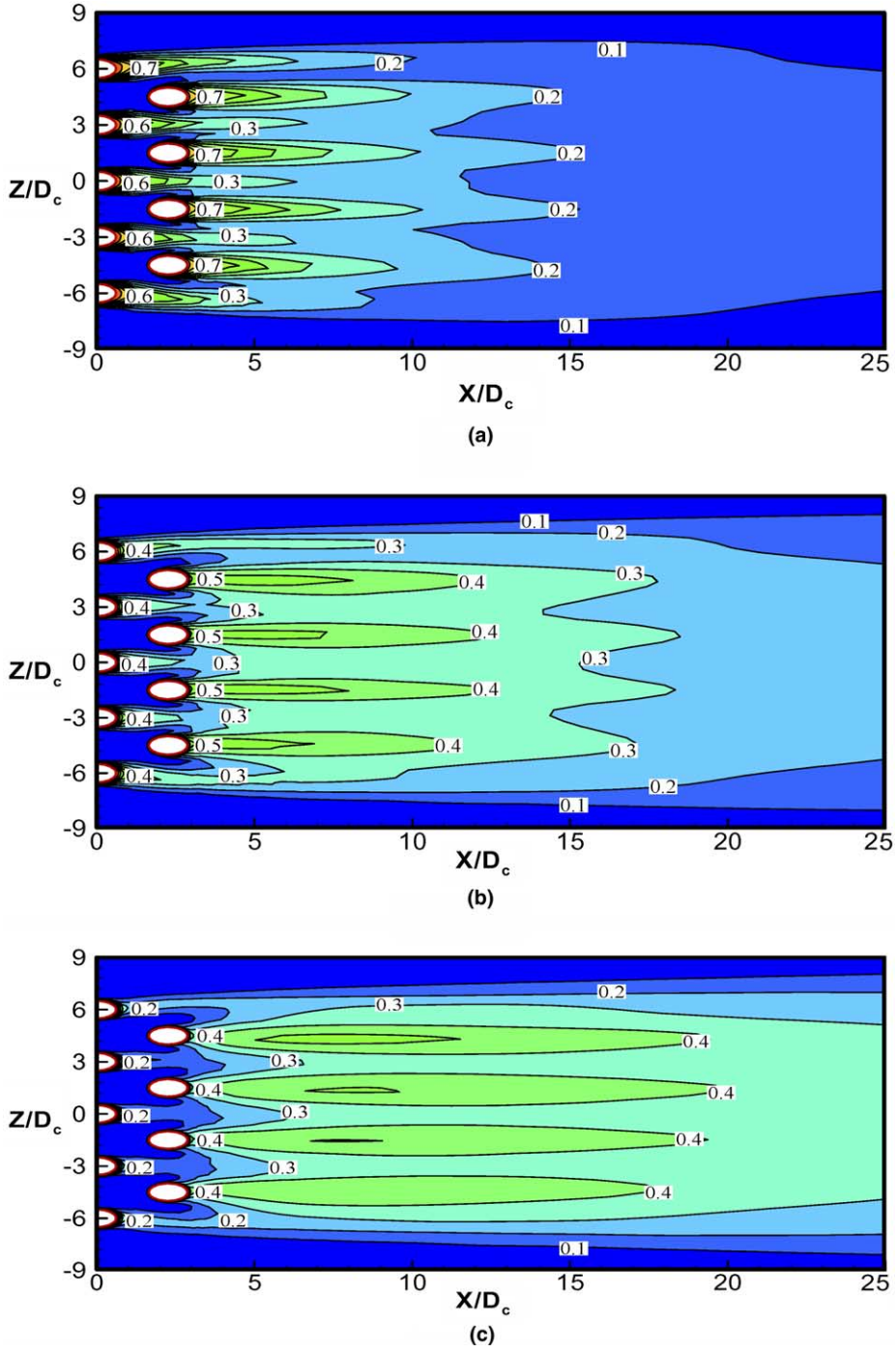

Fig. 16. Effect of blowing ratio on the contours of local adiabatic film cooling effectiveness with model C at $Re = 3440$ for (a) BR = 0.5, (b) BR = 1.0, (c) BR = 1.5.

blown out from each cooling hole to interact with the mainstream. The peak local film-cooling effectiveness obtained for the cross-blow plenum is less than that of the straight-blow plenum for a given blowing ratio downstream of the injections, as determined by comparing Figs. 15 and 16. Figs. 11–14 also indicate that the flow structure of CRVP in cases that involve the cross-blow supply plenum is coherent and stronger than that in cases that involve the straight-blow supply plenum. The same results obtained using models B and D when the angular location of the first row of injection holes is 42°.

3.4. Streamwise distribution of laterally averaged film-cooling effectiveness

The local film-cooling effectiveness is laterally averaged over a pitch of $Z/D_c = \pm 7.5$ to evaluate the effects of the mainstream Reynolds number, the angular location of

the injections and the coolant flow orientation on the lateral spreading of cooling streams. Fig. 17(a) and (b) show the effect of the coolant flow orientation on the streamwise distributions of laterally averaged $\bar{\eta}$ values determined using models A and C, respectively, with various blowing ratios. The tested mainstream Reynolds number is 3440 and the density ratio is 1.14. The cooling holes are on the lateral axis; the hollow arrows indicate the first row of cooling holes and the solid arrows indicate the second. Fig. 17(a) and (b) demonstrate that the effects of the blowing ratio on the $\bar{\eta}$ distributions are similar, independently of the orientation of the coolant flow. At a low blowing ratio, BR = 0.5, the local maximum of the distribution of the curve is governed by the ejection of the cooling stream from the first and second rows of injections. The $\bar{\eta}$ value clearly declines in the direction of the mainstream because of the weak CRVP and the stronger lateral mixing in the direction of the mainstream. When the blowing ratio is at least unity, the lift-off effect of the coolant flow and the strong CRVP flow feature both sharply reduce $\bar{\eta}$ in the region $0 < X/D_c < 10$ for both types of coolant supply plenum. Further downstream, a visible enhancement of $\bar{\eta}$ is observed as the blowing ratio is higher. This is due to reattachment of jet onto the concave wall.

Fig. 18(a) and (b) plot the streamwise distributions of laterally averaged $\bar{\eta}$ values obtained using models B and D, respectively, for various blowing ratios at a fixed Reynolds number of 3440. The first row injections at $X/D_c = 0$ to downstream of $X/D_c = 8$ exhibit a visible difference in laterally averaged $\bar{\eta}$ values at various blowing ratios. Downstream of the injections holes at $0 < X/D_c < 5$, the $\bar{\eta}$ value is maximal at BR = 0.5. In the region $5 < X/D_c < 8$, $\bar{\eta}$ is maximal at BR = 1.0, rather than BR = 0.5. The reattachment of jets on the concave surface leads to an increase in $\bar{\eta}$ farther

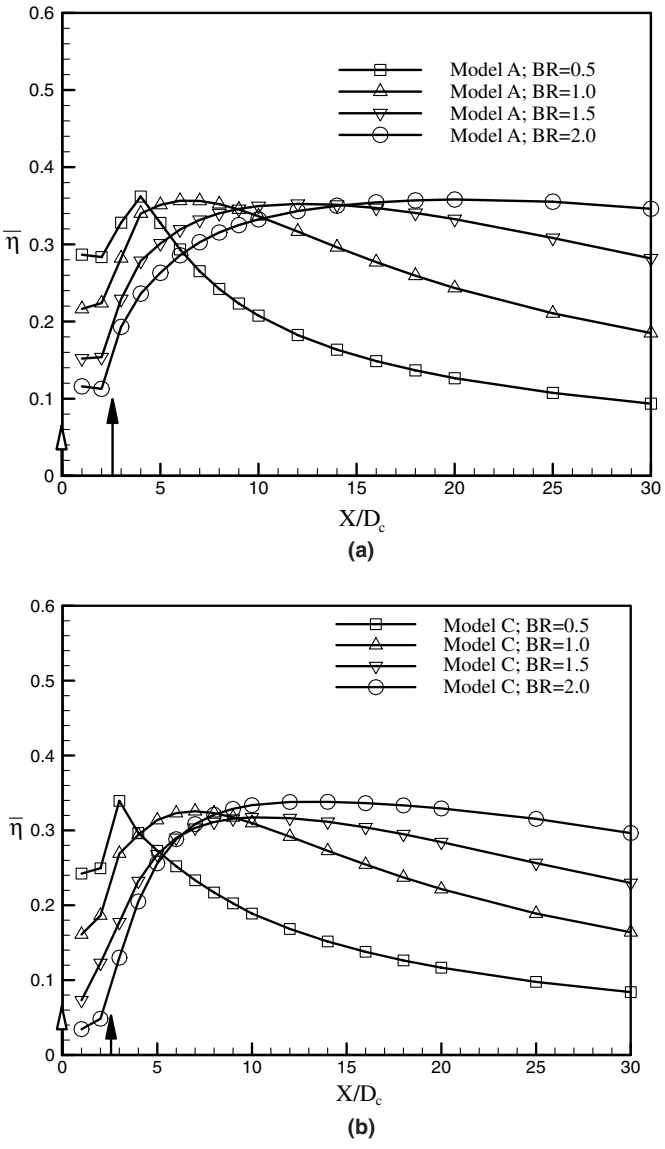

Fig. 17. Effect of blowing ratio on the streamwise distributions of laterally averaged $\bar{\eta}$ value at $Re = 3440$ for (a) model A, (b) model C.

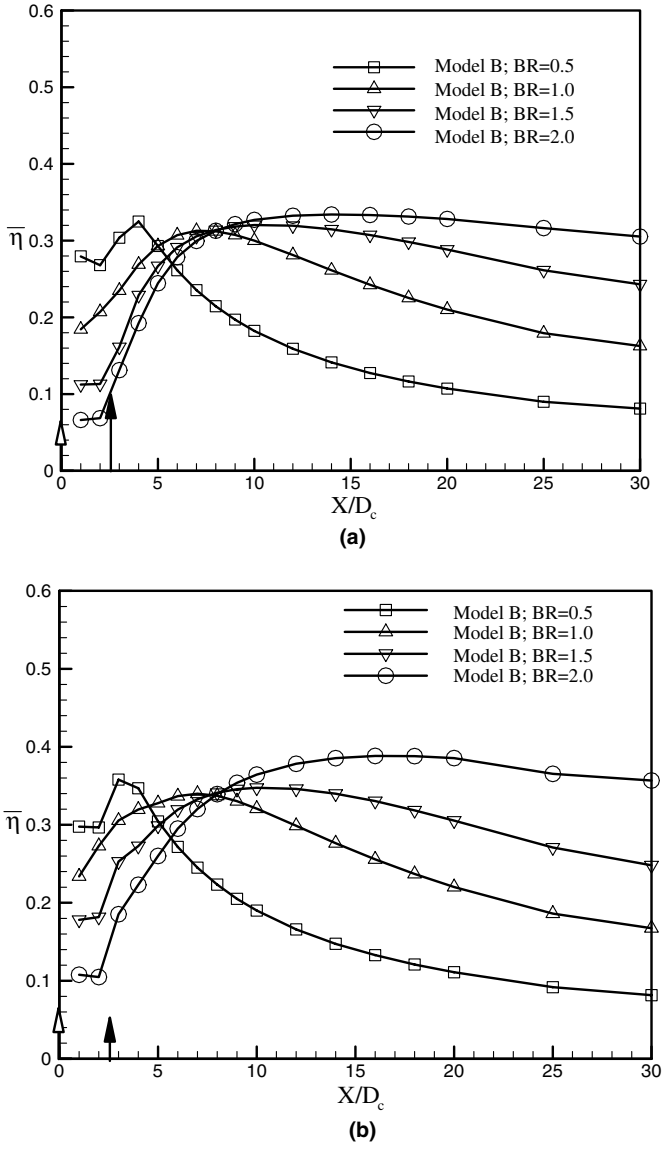

Fig. 18. Effect of blowing ratio on the streamwise distributions of laterally averaged $\bar{\eta}$ value at $Re = 3440$ for (a) model B, (b) model D.

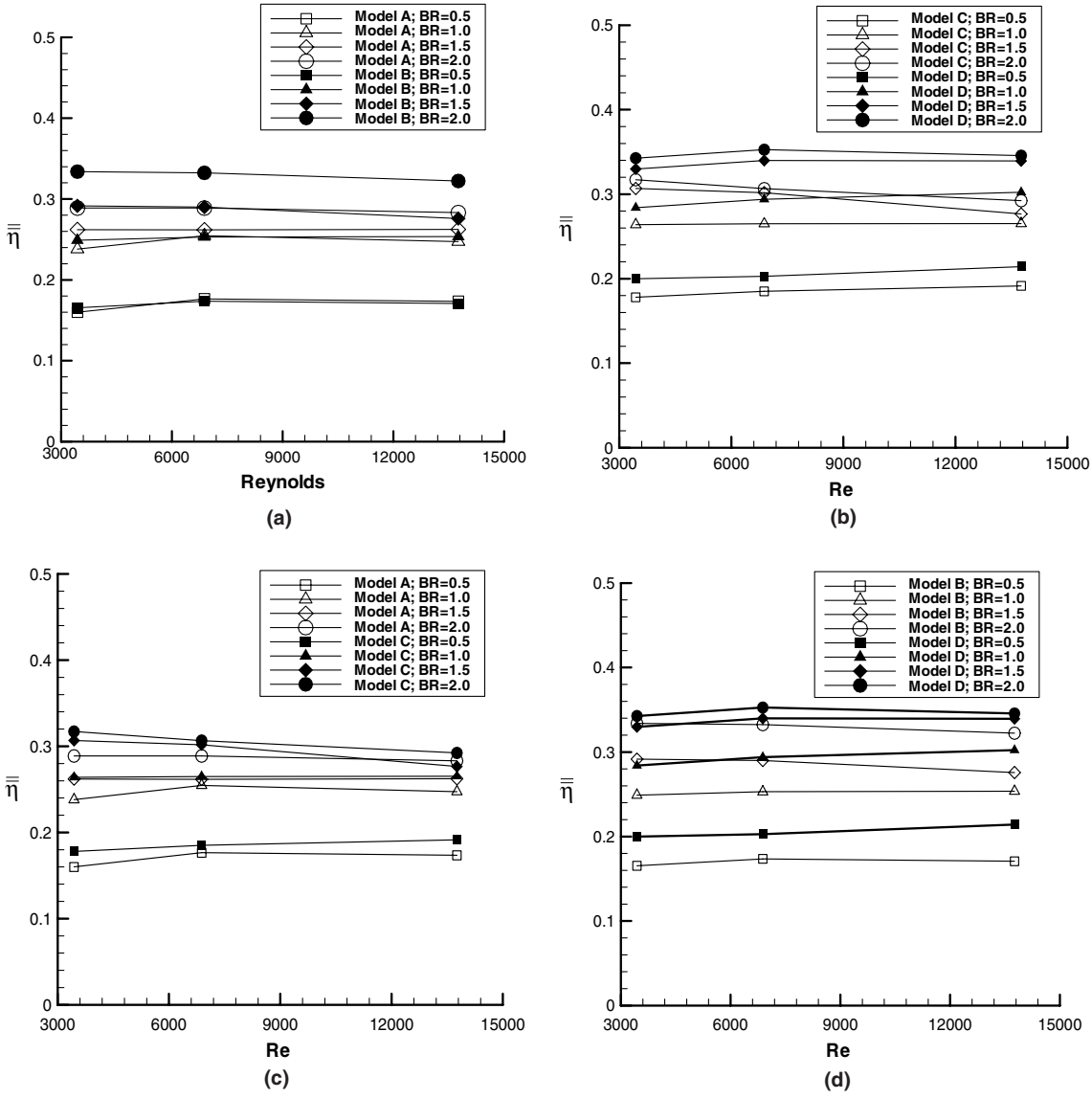

Fig. 19. Effect of mainstream Reynolds number on the $\bar{\bar{\eta}}$ value for (a) models A, B; (b) models C, D; (c) models A, C and (d) models B, D.

downstream at BR = 1.5 and BR = 2.0. In the tested range of blowing ratios, the effect of the angular location of the injections on the distribution of the laterally averaged $\bar{\eta}$ values seems to be essentially insignificant. This insensitivity of the laterally averaged film-cooling effectiveness to the angular location of the injections follows from the stronger mixing effect of the coolant jets and the cross-mainstream over the concave surface.

Fig. 19(a) and (d) reveal the effect of the mainstream Reynolds number on the area-averaged effectiveness $\bar{\bar{\eta}}$ according to models A, B, or C and D at various blowing ratios. A minor variation in $\bar{\bar{\eta}}$ values with *Re* is observed at a given blowing ratio regardless of the model. The $\bar{\bar{\eta}}$ value increased by higher blowing ratio at a given Reynolds number. Fig. 19(a) and (b) also demonstrate that $\bar{\bar{\eta}}$ increases with the angle of the injectant from 40° to 42°, independently of the coolant flow orientation. Fig. 19(c) and (d) present the effect of the coolant flow orientation on $\bar{\bar{\eta}}$ for a fixed the angular location of the injections. Basically, $\bar{\bar{\eta}}$ is higher in cases that involve a straight-blowing plenum than in cases that involve a cross-blowing plenum, over the tested range of blowing ratios.

4. Conclusion

A complete, three-dimensional numerical simulation of a film-cooled concave plate conducted to elucidate the complicated thermal-flow structure features that arise from the jet-in-crossflow problem. The round cooling holes distributed in two rows that each other three times the diameter of a hole. Two coolant flow orientations—straight-blow and cross-blow plenums are tested. The effects of the mainstream Reynolds number, the angular locations of the injections and the blowing ratio on the distributions of effectiveness of cooling of films, are investigated. Some important inferences from the numerical results summarized below:

(1) In this investigation, a multi-block and body-fitted computational grid system that incorporates the mainstream duct, two rows of cooling pipes and a coolant supply plenum was successfully constructed to simulate the complex, thermal-fluid flow field over two rows of a film-cooled concave plate.
(2) The structure of the flowing jet within the coolant pipes affected by both the blowing ratio and the coolant flow orientation. The effects of the angular location of the injections and the mainstream Reynolds number are minor. The coolant flow orientation governs both the trajectory and the lateral spreading of the jet. A pair of in-hole vortices arises near the downstream edge of the holes near the entrance plane of the coolant pipes in cases that involve a straight-blow plenum. However, the internal flow structure of the in-hole velocity field dominated by a single vortical structure around the center of the coolant pipe in the cases of a cross-blow plenum.
(3) The counter-rotating vortex pair (CRVP) clearly observed in both types of coolant plenums over the ranges of mainstream Reynolds numbers and blowing ratios tested. At a particular blowing ratio, the size of the CRVP does not changed significantly, but the jet lifted higher off of the concave surface in the case of the cross-blow plenum. Hence, the laterally averaged film-cooling effectiveness over the concave surface in the case of a straight-blow plenum is slightly higher than that in the case of a cross-blow plenum.
(4) The blowing ratio significantly affects the film-cooling effectiveness. Near the region of jet-crossflow interaction, $\bar{\eta}$ is highest at $BR = 0.5$. Further downstream, $\bar{\eta}$ is highest with $BR = 2.0$, because of the reattachment of jets onto the concave surface.

Acknowledgement

The authors would like to thank the National Science Council of the Republic of China for financially supporting this research under Contract No. NSC 90-2212-E-014-018.

References

[1] R.J. Goldstein, Advances in Heat Transfer, Academic Press, New York, 1971, pp. 321–379.
[2] R.J. Margason, Fifty Years of Jet in Cross-Flow Research, AGARD-CP-534, 1993.
[3] C. Saumweber, A. Schulz, Interaction of film cooling rows: effects of hole geometry and row spacing on the cooling performance downstream of the second row of holes, ASME J. Turbomachinery 126 (2004) 237–246.
[4] R.J. Goldstein, T. Yoshida, The influence of laminar boundary layer and laminar injection on film cooling performance, ASME J. Heat Transfer 104 (1981) 335–362.
[5] R.J. Goldstein, J.R. Taylor, Mass transfer in the neighborhood of jet entering a crossflow, ASME Paper No. 82-HT-62, 1982.
[6] B. Jubran, A. Brown, Film cooling from two rows of hole inclined in the streamwise and spanwise direction, ASME J. Eng. Gas Turbines Power 107 (1985) 84–91.
[7] J.P. Gostelow, G. Hong, N. Melwani, G.J. Mayle, Turbulence-slot development under a moderate adverse pressure gradient, ASME Paper No. 93-GT-377, 1994.
[8] J.P. Bons, C.D. MacArthur, R.B. Rivir, The effect of high free-stream turbulence on film cooling effectiveness, ASME J. Turbomachinery 118 (1996) 814–825.
[9] P.M. Ligrani, A.E. Ramsey, Film cooling from spanwise oriented holes in two staggered rows, ASME Paper No. 95-GT-39, 1995.
[10] S.G. Schwarz, R.J. Goldstein, E.R.G. Eckert, The influence of curvature on film cooling performance, ASME J. Turbomachinery 113 (1991) 472–478.
[11] S.G. Schwarz, Film Cooling of Curved Surfaces, Ph.D. thesis, University of Minnesota, Minneapolis, MN, 1986.
[12] P.H. Chen, P.P. Ding, D. Ai, An improved data reduction method for transient liquid crystal thermography on film cooling measurements, Int. J. Heat Mass Transfer 44 (2001) 1379–1387.
[13] D.K. Walters, J.H. Leylek, A detailed analysis of film cooling physics. Part I: streamwise injection with cylindrical holes, ASME Paper 97-GT-269, 1997.
[14] M.K. Berhe, S.V. Patankar, Curvature effects on discrete hole film cooling, ASME J. Turbomachinery 121 (1999) 781–791.
[15] V.K. Garg, R.E. Gaugler, Effect of velocity and temperature distribution at the hole exit on film cooling of turbine blades, ASME J. Turbomachinery 119 (1997) 343–351.
[16] S.D. Peterson, M.W. Plesniak, Short-hole jet-in-crossflow velocity field and its relationship to film-cooling performance, Exp. Fluids 33 (2002) 89–898.
[17] S. Wittig, A. Schulz, M. Gritsch, K.A. Thole, Transonic film-cooling investigations: effects of hole shapes and orientations, ASME Paper No. 96-GT-222, 1996.
[18] B.Y. Maiteh, B.A. Jubran, Effects of pressure gradient on film cooling effectiveness from two rows of simple and compound angle holes in combination, Energy Convers. Manage. 45 (2004) 1457–1469.